DOI: 10.61782/fa.2025.0214

COMMUNITY AND CABIN NOISE ASSESSMENT OF A 19-SEATER HYDROGEN-ELECTRIC AIRLINER

Mattia Barbarino[1*] **Giovanni Fasulo**[1] **Antonio Pagano**[1] **Antonio Visingardi**[1]
Fabrizio Morlando[1] **Francesco Petrosino**[1] **Miha Zupanič**[2] **Jernej Drofelnik**[2]

[1] Italian Aerospace Research Centre (CIRA), Via Maiorise, 81043, Capua (CE), Italy
[2] Pipistrel Vertical Solutions d.o.o, Vipavska cesta 2, 5270 Ajdovščina, Slovenia

ABSTRACT

The need to reduce the environmental impact of aviation, as envisaged by Europe's Flightpath 2050 vision, is pushing the development of sustainable and cost-efficient air mobility solutions. Within this framework, the European project NEWBORN is developing hybrid and full electric powertrains. For the latter, which combines hydrogen fuel cells and batteries for aeronautical applications, demonstrations are also planned on representative CS23 and CS25 aircraft platforms. This paper assesses the environmental performance and cabin noise characteristics of the innovative "Miniliner", a 19-passenger airliner equipped with the NEWBORN-developed propulsion system whose propulsors are two newly designed propellers. The rotational movement of propellers (co-rotating and counter-rotating) is examined considering the setup options (including direction of rotation and blade phase shift). The results of a comprehensive numerical framework are analyzed shedding light on the optimal propeller arrangement to reduce both external and cabin noise levels.

Keywords: *newborn, aeroacoustic, synchrophasing, hybrid aircraft.*

**Corresponding author: M.Barbarino@cira.it.*

1. INTRODUCTION

Hydrogen fuel cell and battery technologies promise to revolutionize sustainable aviation by delivering zero in-flight emissions and substantially reducing the environmental footprint of air transport [1–3]. Reflecting this potential, the EU-funded NEWBORN project [4] brings together 18 partners from 10 European countries in an ambitious effort to mature and optimize advanced technologies. The project aims to support an EIS for CS-23 aircraft by 2030 and regional aircraft by 2035, making it imperative to address both environmental and cabin noise impacts in order to meet increasingly stringent noise regulations and enhance passenger comfort. In this context, the present paper investigates an innovative 19-passenger airliner, the "Miniliner", an aircraft equipped with a fuel cell-battery power system.

In turboprop aircraft, the primary noise source are the propeller blades, and cabin noise levels typically exceed those of commercial jets by 10 to 30 decibels due to dominant low-frequency tones [5]. To mitigate these challenges, three distinct propeller configurations were initially analyzed: co-rotating propellers, counter-rotating propellers with the outer blades moving upward, and counter-rotating propellers with the outer blades moving downward. Moreover, given the possible integration of a synchrophasing system, which should be capable of comparing and adjusting the azimuthal positions of the propellers, the influence of relative phase shifts on both external and cabin noise levels was examined. Specifically, the adopted methodology encompasses the development of a propeller design based on top-level aircraft requirements, followed by comprehensive aerodynamic and aeroacoustic analyses of the full aircraft under various flight conditions. Finally, finite element models of the aircraft's structure and fuselage interior cavities were developed for direct frequency vibro-acoustic analysis. Recognizing that the low-frequency acoustic field within the cabin is highly sensitive to observer position, and consequently, that each passenger experiences different levels of acoustic comfort, the optimal propeller phase shift was determined by averaging the acoustic level across a plane at the height of seated passengers' ears. For external noise, the optimization target was a 3 m × 3 m area around the ICAO certification point, with the aim of redistributing noise to lower levels at this critical location and thereby supporting the aircraft's acoustic certification process.

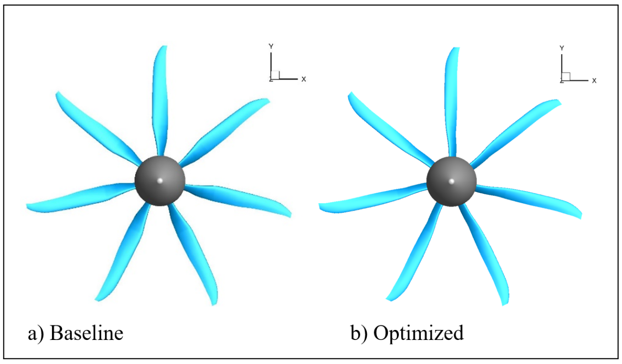

Figure 1. Propeller design.

2. PROPELLER NOISE ESTIMATION

2.1 Propeller Design

The propeller was entirely designed and optimized by CIRA and features a seven-blade configuration with a diameter of 3.2 m (Figure 1). The design process was structured in three distinct phases: generation of the preliminary blade shape, refinement through DOE, and final multi-objective optimization. Initially, a method inspired by Adkins and Liebeck [6] was employed to establish the chord and twist distributions under take-off conditions. The geometry's potential was then assessed using a DOE that defines low and high bounds for the design variables, thereby delineating a restricted design space. Within this space, a multi-objective optimization seeks the optimal compromise in the blade planform to enhance propeller performance during both take-off and cruise. Two CIRA in-house tools based on Blade Element Momentum Theory (BEMT) support this first phase: one serves as a design tool using a preset airfoil lift coefficient distribution, while the other provides analysis and trim by extracting aerodynamic blade sectional properties from airfoil lookup tables. As the design of the airfoil family is beyond the project's scope, CIRA proprietary airfoil geometries are utilized. The entire multidisciplinary numerical process is implemented within the commercial optimization environment Optimus [7], with performance evaluation conducted via a dedicated BEMT code for propeller analysis and trim.

2.2 Aerodynamic Simulations

To predict the noise generated by the aircraft under various flight conditions, aerodynamic simulations were performed to generate a database of unsteady surface pressure distributions. Initially, the geometry of the CS23 regional aircraft was discretized using a structured surface mesh generated in Pointwise® [8], employing nine patches and resulting in a total of 7750 panels. Each blade geometry was subsequently discretized into 60 chordwise panels by 26 spanwise panels using the same commercial software. Numerical simulations were then executed with the RAMSYS code [9], an unsteady, inviscid, and incompressible free-wake vortex lattice boundary element method (BEM) solver developed at CIRA for multi-rotor, multi-body configurations. This code is based on Morino's boundary integral formulation for solving Laplace's equation for the velocity potential. Surface pressure distributions were computed by applying the unsteady Bernoulli equation, and the resulting pressures were integrated to obtain the forces and moments on both the configuration and adjacent obstacles. The simulations were carried out under nine distinct test conditions that represent key mission segments, including taxi, take-off, climb, cruise, and descent, and considered three different propeller configurations:

1. Co-rotating propellers (CRP): the propellers rotate counter-clockwise when viewed from the aircraft's front (Figure 2a).
2. Counter-rotating propellers outer blades upward (CTRP-U): the outer blades of both propellers move upward (Figure 2b).
3. Counter-rotating propellers outer blades downward (CTRP-D): the outer blades of both propellers move downward (Figure 2c).

The aerodynamic simulations used a time discretiza-

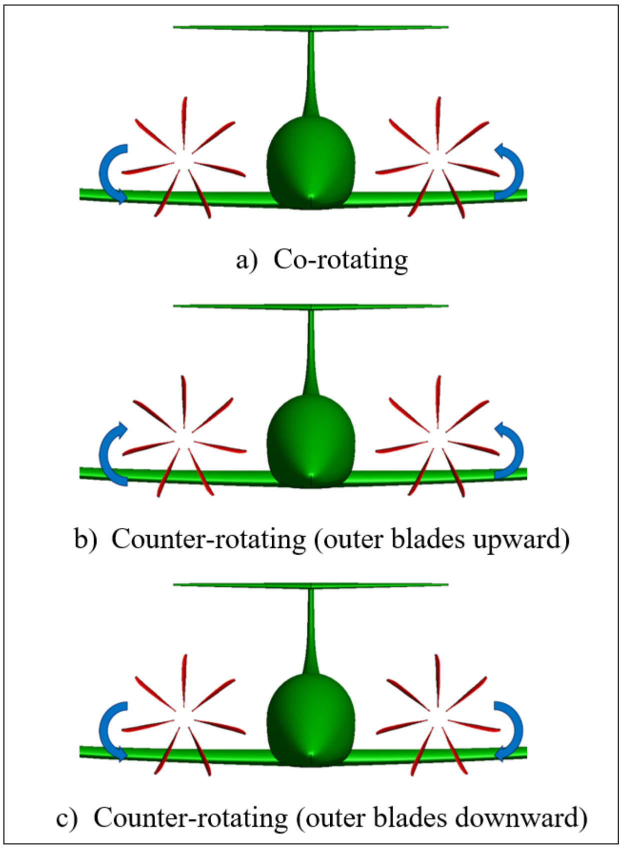

Figure 2. Rotational directions propellers.

tion corresponding to an azimuth step of 2°. Four wake spirals were modeled, and four rotor revolutions were required to achieve a converged periodic solution for all test cases, with the taxi condition being the only exception, requiring six wake spirals and six rotor revolutions. Figure 3 illustrates an example of the wake system development during cruise flight after four revolutions, highlighting the interaction between the propellers, their wakes, and the airframe.

2.3 Aeroacoustic Simulations

The acoustic free-field generated by the propellers was computed using the ACO-FWH solver, which utilizes as input the aerodynamic database comprising rotor blade pressure distributions. The solver is based on the Ffowcs Williams-Hawkings (FW-H) formulation [10] as detailed in [11–13]. The advanced-time formulation of Farassat 1A was employed, and the linear terms (the so-called

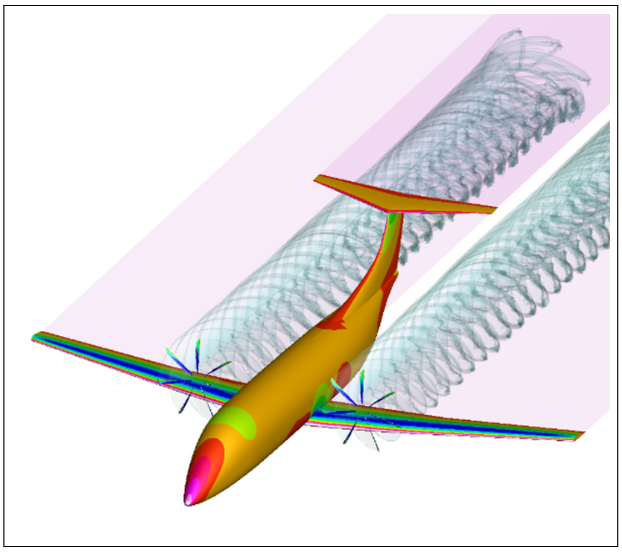

Figure 3. The aircraft with co-rotating propellers and its wake system.

thickness and loading noise contributions) were computed through integrals on the moving blade surfaces (impermeable/rigid surface formulation). Computational acceleration was achieved via parallel execution using the MPI API.

2.4 Vibroacoustic Simulations

To predict cabin noise, a fully coupled vibroacoustic analysis was required to capture the interactions between structural and acoustic natural modes, particularly near the first harmonic of the Blade Passage Frequency (BPF). This was achieved through a Direct Frequency Response analysis on a model that integrates both the fuselage airframe and the acoustic passenger cabin, with the propeller-generated pressure field applied to the airframe's external surface. The analysis was performed using MSC NASTRAN [14], where the pressure field was converted into nodal forces on the 2D shell elements representing the airframe skin. To preserve both amplitude and phase information, DAREA and DPHASE cards were employed for accurate force allocation. Furthermore, the full coupling analysis was automatically configured by including an ACMODL card in the NASTRAN bulk data input file, with non-coincident conditions imposed at the structure-fluid coupling interfaces.

A comprehensive structural FEM of the entire aircraft fuselage was developed using an automated process.

The airframe skin was discretized with two-dimensional shell elements, while the reinforcement components, axial stringers (L-section) and circumferential frames (Z-section), were modeled with one-dimensional, uniformly spaced elements, both made of aluminum. The floor was represented by an equivalent isotropic and homogeneous material to mimic a lightweight, thick foam sandwich, also using two-dimensional shell elements. Its reinforcement system comprises a grid of beams: C-section beams deployed transversely and I-section beams along the longitudinal axis, with additional circular-section beams connecting the floor to the fuselage's stiffening system. The structural mesh size was chosen to accurately capture the bending wavelength at the highest frequency investigated for the most flexible component (the airframe skin), adhering to the guideline of 6 to 10 linear elements per wavelength, resulting in an approximate mesh size of 2 cm. Furthermore, an acoustic FEM was developed to model the fuselage's primary interior cavities: the cabin and the cargo area. Given the linear relationship between frequency and wavelength, and assuming 10 elements per wavelength, a speed of sound of 340 m/s, and a maximum frequency of 500 Hz, the minimum acoustic element size was set to approximately 7 cm.

A modal analysis was then performed to ensure that the whole model was correctly assembled. For simplicity, the first natural frequencies for the structure, the cabin volume, and the cargo volume were reported.

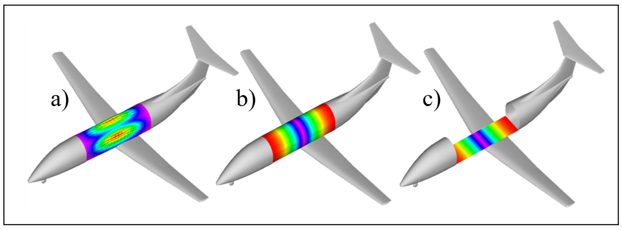

Figure 4. First natural frequency of: a) structural model - 60.3 Hz; b) cabin acoustic model - 25.8 Hz; c) cargo acoustic model - 25.8 Hz.

3. RESULTS

3.1 External Noise

This section examines the take-off noise produced by the two propellers. The noise was computed over a 3 m x 3 m ground area centered on the ICAO certification point (Figure 5). Averaged values of A-weighted Sound Exposure Level (A-SEL) and Effective Perceived Noise Level (EPNL) were selected as the noise metrics to compute. In compliance with ICAO Annex 16, the use of EPNL (based on Miniliner's weight category) provides the basis for assessing the noise performance and obtain the certification.

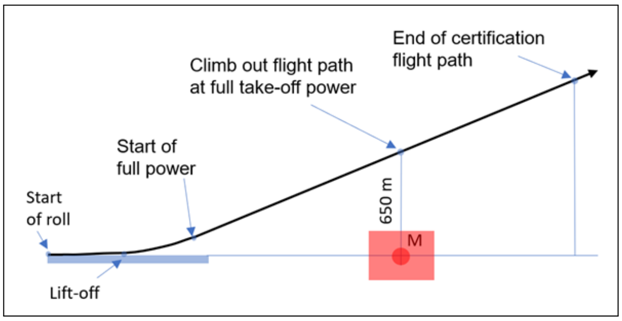

Figure 5. Take-off trajectory and the designated 3 m x 3 m area surrounding the ICAO certification point (red square).

Figure 6 illustrates the tonal noise propagated to the ground, showing the EPNL for both propellers across the three analyzed configurations (CRP, CTRP-D and CTRP-U).

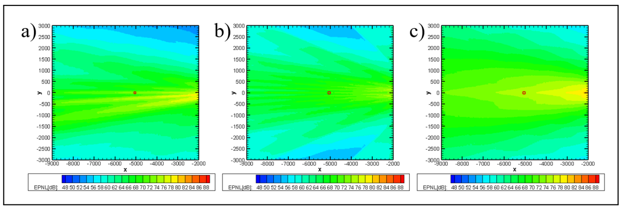

Figure 6. Contour of EPNL for tonal noise from: a) co-rotating propellers; b) counter-rotating down propellers; c) counter-rotating up propellers.

Analysis of these results indicates that the contra-rotating up configuration increases the EPNL at the certification point, while the contra-rotating down configuration achieves the greatest reduction at the certification point (approximately -1.6 dB). Meanwhile, the co-rotating configuration represents a balanced solution in terms of both A-SEL and EPNL.

3.2 Cabin Noise

Concerning cabin noise, the low-frequency acoustic field is highly sensitive to the observer's position, resulting in variable acoustic comfort among passengers. To address this issue, the study aims to compute metrics that provides a balanced acoustic environment for all occupants. Specifically, a measurement plane at a height of 1.2 m from the floor, corresponding to the ear level of seated passengers, was selected to compute both the maximum A-weighted Overall Sound Pressure Level (A-OASPL) and the mean A-weighted OASPL (Figure 7).

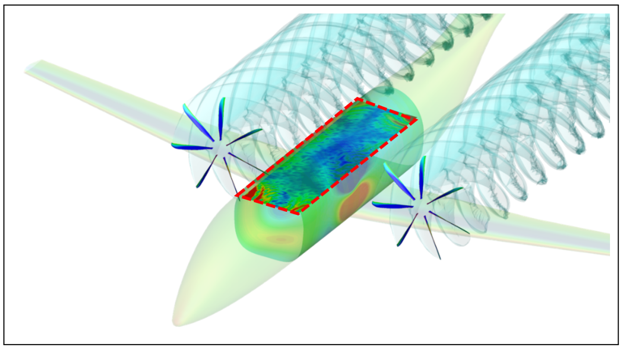

Figure 7. Selected plane for the cabin noise estimation.

Since the first harmonic of the BPF predominantly contributes to cabin noise levels, the analysis focused exclusively on the response at this frequency. Figure 8 presents the A-OASPL within the cabin, measured on a recovery plane positioned at a height of 1.2 m for all three configurations (CRP, CTRP-D and CTRP-U). Notably, the acoustic load was calculated under the assumption that the propellers operated in cruise conditions.

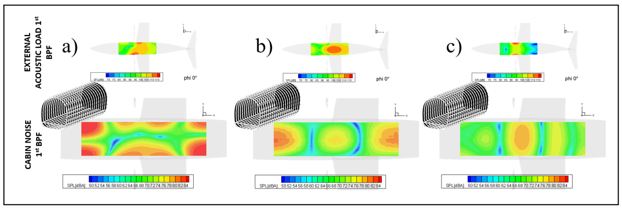

Figure 8. Cabin A-OASPL contour at the first harmonic of the BPF from: a) co-rotating propellers; b) counter-rotating down propellers; c) counter-rotating up propellers.

Analysis of these single value metrics reveals that the co-rotating configuration generates the most disruptive noise conditions, whereas the contra-rotating down configuration yields a modest reduction in cabin noise. Notably, the contra-rotating up configuration significantly decreases cabin noise, improving the mean A-OASPL by up to 7 dBA.

Figure 9 summarizes the results for both cabin and external noise across the three analyzed configurations.

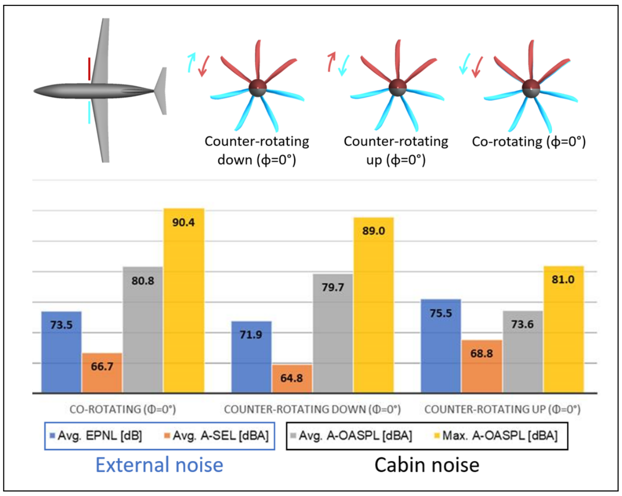

Figure 9. External and cabin noise from propellers under various configurations.

3.3 Synchrophasing

This section details the optimization of the synchrophasing system for the Miniliner configuration. The primary aim was to identify the optimal propeller phase shift for each of the three analyzed configurations (CRP, CTRP-D and CTRP-U) in order to mitigate both cabin and external noise for certification purposes. A phase shift grid was established spanning from 0° to 50°. Aerodynamic, aeroacoustic, and vibroacoustic analyses were executed automatically via a dedicated script. For each discrete phase shift value, the noise metrics defined in earlier subsections were computed. Then, to refine the resolution beyond the initial simulation grid, spline interpolation was employed, providing more precise estimates of the noise metrics and a smoother representation of the trends. Subsequently, an objective function was formulated to minimize overall noise. This function integrates internal and external noise metrics: internal noise is quantified by the average A-OASPL across the cabin plane at 1.2 m from the floor, while external noise is characterized by the average EPNL over a 3 m × 3 m area around the ICAO certification point. Given the differing scales of these metrics, each was normalized by its mean value computed over the entire 0°-50° range, ensuring a balanced contribution within the objective function. Three weighting schemes were evaluated to explore distinct noise reduction strategies:

1. 100% cabin noise focus: prioritizes the reduction of internal noise exclusively.

2. 100% external noise focus: targets the reduction of external noise exclusively.

3. Balanced (50% cabin, 50% external): provides an equilibrium solution that simultaneously reduces both internal and external noise.

As expected, the optimal angle varies depending on whether the primary objective is to reduce cabin noise or external noise. It should be noted that external noise was evaluated over a 3 m × 3 m area surrounding the certification point and should not be interpreted as the absolute reduction in total external noise: certain configurations may exhibit advantages specifically at the certification level. Specifically, for the co-rotating propellers configuration, a dephasing angle of approximately 25° achieved the maximum reduction in both cabin and external noise when compared to the zero-dephasing case. In contrast, in the case of the counter-rotating up propellers configuration, the objectives of reducing cabin and external noise are in conflict. In fact, the dephasing angle that minimizes airport noise would result in an approximate increase of 8 dBA in average cabin noise, an outcome deemed unacceptable. Consequently, the zero-dephasing configuration was selected as the optimal choice for this configuration. Finally, for the counter-rotating down propellers configuration, a dephasing angle of approximately 25° produced the greatest reduction in external noise relative to the zero-dephasing configuration. Although this angle led to a modest increase of 1 dBA in cabin noise, no alternative dephasing angles provided any significant improvement in internal noise levels. Therefore, 25° is justified as the optimal choice for this setup. The comparative results are summarized in the bar graph presented in Figure 10, which also includes the baseline configuration for the co-rotating propeller without any dephasing angle.

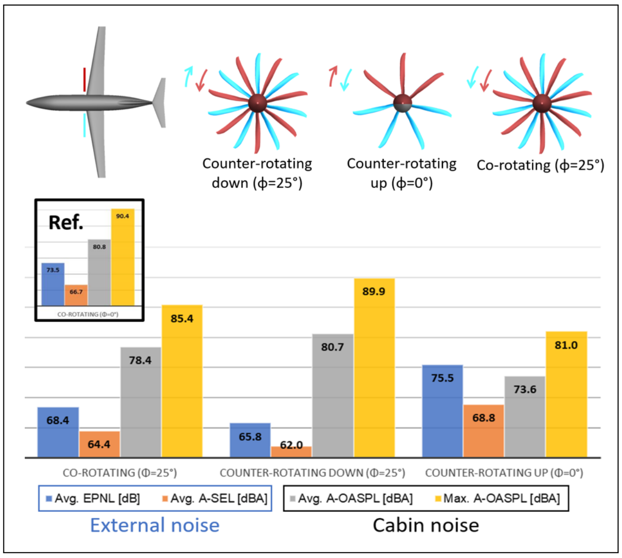

Figure 10. External and cabin noise from propellers under various configurations operating at their optimal dephasing angle.

4. CONCLUSIONS

Within the NEWBORN project framework, a comprehensive procedure was implemented to evaluate noise impacts on a next-generation air mobility concept. The study focused on the innovative Miniliner, a 19-passenger airliner powered by a propulsion system that integrates hydrogen fuel cells and batteries, to assess both environmental performance and cabin noise. The approach combined four key components: propeller design, aerodynamic, aeroacoustic and vibroacoustic simulations. Initially, a multi-objective optimization strategy was applied during the propeller design phase to balance performance across varied flight conditions. Detailed aerodynamic simulations then provided unsteady pressure distributions, which were used with an FW-H based method to compute the aircraft's acoustic signature. Finally, a vibroacoustic analysis, accounting for the coupled behavior of the airframe and cabin, enabled the accurate prediction of cabin noise levels. The study specifically analyzed take-off noise produced by the propellers. For this purpose, a 3 m × 3 m ground area centered on the ICAO certification point was considered to calculate the mean A-weighted Sound Exposure Level and mean Effective Perceived Noise Level. In parallel, cabin noise was assessed on a measurement plane set 1.2 m above the floor, mimicking the ear level of seated passengers, to determine both the maximum and mean A-weighted Overall Sound Pressure Level. Three different propeller configurations were compared for both external and internal noise assessment:

- Counter-rotating with outer blades downward: this setup notably reduces external noise, though it only modestly decreases cabin noise.
- Counter-rotating with outer blades upward: this configuration significantly lowers cabin noise but is associated with higher external noise levels.
- Co-rotating: this option results in the highest cabin noise, yet it maintains a balanced level of external noise.

The phase shift angle optimization between the two seven-bladed, synchro-rotating propellers was performed for each of the three propeller configurations. Specifically, the counter-rotating down configuration, with a dephasing angle of 25°, provided the most effective reduction in external noise. In contrast, the counter-rotating up configuration, when operated at its optimal dephasing angle of 0°, achieved the greatest reduction in cabin noise, although at the expense of external noise performance. Whereas, a balanced solution that offers moderate reductions in both cabin and external noise can be provided by the co-rotating configuration with a dephasing angle of 25°.

The insights derived from this analysis are intended to inform subsequent phases of the research. Future work, featuring more detailed performance evaluations, will help refine these conclusions and support the broader implementation of this findings in the aviation industry.

5. ACKNOWLEDGMENTS

This research was funded by the European Union's Horizon research and innovation programme under grant agreement No. 101101967, project NEWBORN (NExt generation high poWer fuel cells for airBORNe applications).

6. REFERENCES

[1] T. Yusaf, A. S. F. Mahamude, K. Kadirgama, D. Ramasamy, K. Farhana, H. A. Dhahad, and A. R. A. Talib, "Sustainable hydrogen energy in aviation–a narrative review," *International Journal of Hydrogen Energy*, vol. 52, pp. 1026–1045, 2024.

[2] S. Tiwari, M. J. Pekris, and J. J. Doherty, "A review of liquid hydrogen aircraft and propulsion technologies," *International Journal of Hydrogen Energy*, vol. 57, pp. 1174–1196, 2024.

[3] E. J. Adler and J. R. Martins, "Hydrogen-powered aircraft: Fundamental concepts, key technologies, and environmental impacts," *Progress in Aerospace Sciences*, vol. 141, p. 100922, 2023.

[4] E. Commission, "Next generation high power fuel cells for airborne applications (newborn)," tech. rep., CORDIS, 2023. Project Report. `https://cordis.europa.eu/project/id/101101967/reporting`.

[5] M. Barbarino, P. Vitiello, R. Lombardi, and A. Pagano, "Optimized synchrophasing system of a turbo-prop aircraft for cabin noise reduction," in *INTER-NOISE and NOISE-CON Congress and Conference Proceedings*, vol. 259, pp. 4752–4759, Institute of Noise Control Engineering, 2019.

[6] C. Adkins and R. Liebeck, "Design of optimum propellers," *Journal of Propulsion and Power*, vol. 10, Sept-Oct 1994.

[7] N. solutions, "Optimus 2020.1." `http://www.noesissolutions.com`, 2020.

[8] "Pointwise®." `https://www.pointwise.com`. Accessed: 24 March 2025.

[9] A. Visingardi, A. D'Alascio, A. Pagano, and P. Renzoni, "Validation of cira's rotorcraft aerodynamic modelling system with dnw experimental data," in *22nd European Rotorcraft Forum*, (Brighton, UK), 1996.

[10] J. E. F. Williams and D. L. Hawkings, "Sound generation by turbulence and surfaces in arbitrary motion," *Philosophical Transactions of the Royal Society of London. Series A, Mathematical and Physical Sciences*, vol. 264, no. 1151, pp. 321–342, 1969.

[11] D. Casalino, "An advanced time approach for acoustic analogy predictions," *Journal of Sound and Vibration*, vol. 261, no. 4, pp. 583–612, 2003.

[12] D. Casalino, M. Barbarino, and A. Visingardi, "Simulation of helicopter community noise in complex urban geometry," *AIAA Journal*, vol. 49, no. 8, pp. 1614–1624, 2011.

[13] M. Barbarino, F. Petrosino, and A. Visingardi, "A high-fidelity aeroacoustic simulation of a vtol aircraft in an urban air mobility scenario," *Aerospace Science and Technology*, p. 107104, 2021.

[14] Hexagon, *MSC Nastran 2022.2 Getting Started Guide*, 2022.